NRC Research Press

ARTICLE

A novel hydrogen-bonded organic framework for the sensing of two representative organic arsenics

Ting Liu, Bin Wang, Ru He, Hadi Arman, Kirk S. Schanze, Shengchang Xiang, Dan Li, and Banglin Chen

Abstract: A novel fluorescent hydrogen-bonded organic framework with a double fold interpenetrated structure, HOF-22, has been successfully constructed and structurally characterized. HOF-22 is capable of sensitive detection of two representative organic arsenics from aqueous solution.

Key words: hydrogen-bonded organic frameworks (HOFs), sensing, fluorescence quenching, organic arsenics.

Résumé : Nous avons construit un nouveau réseau organique à liaisons hydrogène fluorescent comportant une structure à deux motifs interpénétrés, le réseau HOF-22, et avons caractérisé sa structure. Nous avons ensuite démontré que HOF-22 peut être utilisé pour effectuer la détection sensible en solution aqueuse de deux composés organiques d'arsenic représentatifs. [Traduit par la Rédaction]

Mots-clés : réseaux organiques à liaisons hydrogène (HOF), détection, extinction de fluorescence, composés organiques d'arsenic.

Introduction

Hydrogen-bonded organic frameworks (HOFs) are a kind of crystalline porous solid constructed by organic building units (OBUs) through hydrogen bonding interactions.[1,2] Similar with other famous porous materials like metal-organic frameworks (MOFs)[3–7] and zeolitic imidazolate frameworks (ZIFs),[8,9] HOFs also attracted much attention because of their large surface area, high porosity, tailored pore size, and predictable structure.[10–12] Recently, many HOFs have been reported with promising applications in gas storage and separation,[13–16] chemical sensing,[17–21] proton conduction,[22–24] photodynamic therapy,[25] and so on. Besides, HOFs have their unique features. For example, HOFs are soluble and can be purified and recycled easily by simple recrystallization due to the features of weak non-covalent interactions. The metal-free nature endows HOFs low density, low toxicity, and considerable biocompatibility; thus, they can act as an excellent candidate in biological application.[26]

Due to the very weak interactions between linkers, it is difficult to obtain a three-dimensional (3D) supramolecular structure with high porosity. Moreover, the low rigidity and directionality of hydrogen bonds make it more challenging to design and construct porous HOFs. These issues have severely obstructed the development and practical application of HOF materials. To solve this problem, many well-designed supramolecular synthons[17,27,28] have been employed such as carboxylic acid,[10,25] pyrazole,[11,29,30] 2,4-diaminotriazine,[31–37] amide,[38] pyridine,[39] and so on. Among them, carboxylic acid can form a rigid and directional carboxylic acid···carboxylic acid dimeric H-bonding unit, which is more promising for the construction of porous HOFs. To date, several OBUs with carboxylic acid synthons have been reported; most of them, however, are based on tetra- and hexa-carboxylic acids. Tricarboxylic acids have been rarely reported for the construction of HOFs.[14,15,40–42]

Herein, a novel 2-fold interpenetrated fluorescent 3D HOF, HOF-22, has been successfully constructed from a tri-carboxylic acid OBU, 5′-(4-carboxyphenyl)-2′,4′,6′-trimethyl-[1,1′:3′,1″-terphenyl]-4,4″-dicarboxylic acid (H_3CTTA), by simple recrystallization in ethanol (Scheme 1). HOF-22 can be used as a fluorescent sensor for the efficient detection of two representative organic arsenics, roxarsone (ROX) and nitarsone (NIT), from aqueous solution.

Experimental

Materials and instruments

All general reagents and solvents (AR grade) were commercially available and used as received. Powder X-ray diffraction (PXRD) data were recorded on a Rigaku Smartlab3 X-ray powder diffractometer equipped with a Cu sealed tube (λ = 1.54178 Å) at room temperature. Thermogravimetric analyses (TGA) were performed under nitrogen with a heating rate of 10 °C min^{-1} on TGA-50 (Shimadzu) thermogravimetric analyzer. Fluorescence measurements were made on an Edinburgh Instruments FLS-1000 fluorescence spectrophotometer. UV–vis spectra were obtained with a UV-2600 spectrophotometer in the range of 250–800 nm at room temperature.

Received 4 November 2019. Accepted 22 January 2020.

T. Liu. College of Chemistry and Materials Science, Jinan University, Guangzhou 510632, P.R. China; Department of Chemistry, University of Texas at San Antonio, 1 UTSA Circle, San Antonio, TX 78249-0698, USA.
B. Wang. Department of Chemistry, University of Texas at San Antonio, 1 UTSA Circle, San Antonio, TX 78249-0698, USA; Fujian Provincial Key Laboratory of Polymer Materials, College of Chemistry and Materials Science, Fujian Normal University, 32 Shangsan Road, Fuzhou 350007, P.R. China.
R. He and K.S. Schanze. Department of Chemistry, University of Florida, Gainesville, FL 32611, USA.
H. Arman and B. Chen. Department of Chemistry, University of Texas at San Antonio, 1 UTSA Circle, San Antonio, TX 78249-0698, USA.
S. Xiang. Fujian Provincial Key Laboratory of Polymer Materials, College of Chemistry and Materials Science, Fujian Normal University, 32 Shangsan Road, Fuzhou 350007, P.R. China.
D. Li. College of Chemistry and Materials Science, Jinan University, Guangzhou 510632, P.R. China.
Corresponding authors: Bin Wang (email: bin.wang@utsa.edu), Dan Li (email: danli@jnu.edu.cn), and Banglin Chen (email: banglin.chen@utsa.edu).
This paper is part of a special issue to honour Professor Jim Wuest.

Published at www.nrcresearchpress.com/cjc on 11 February 2020.

Scheme 1. Chemical drawing of H_3CTTA.

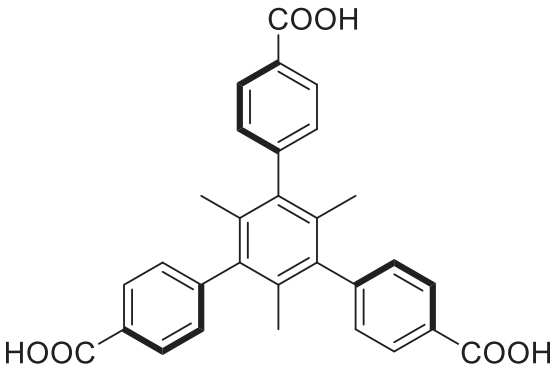

Synthesis

The organic building unit H_3CTTA was synthesized according to a literature method.[43] The detailed description is provided in the Supplementary data.

HOF-22

Colourless needle crystals of HOF-22 were obtained by slow evaporation of the solution of 3 mg H_3CTTA in 2 mL EtOH over a period of 2 days. The obtained single crystals were collected and air-dried for further use.

Single-crystal X-ray diffraction

The crystal data of HOF-22 were collected on a Rigaku supernova X-ray diffractometer equipped with a graphite-monochromatic enhanced Cu Kα radiation (λ = 1.54184 Å) at 100 K. The datasets were corrected by empirical absorption correction using spherical harmonics, implemented in the SCALE3 ABSPACk scaling algorithm. The structure of HOF-22 was solved by direct methods and refined by full-matrix least-squares on F^2 with anisotropic displacement using the SHELXTL software package.[44] Non-hydrogen atoms were refined with anisotropic displacement parameters during the final cycles. Hydrogen atoms of the ligands were calculated in ideal positions with isotropic displacement parameters. The details of structural refinement can be found in Table 1 and the cif file.

Fluorescence measurements

The finely grounded powder sample of HOF-22 (3 mg) was immersed in 20 mL of H_2O and ultrasonicated for 10 min to form a stable turbid suspension and then 1 mL of it was added to a cuvette. The fluorescence upon excitation at 300 nm of HOF-22 was measured in-situ after incremental addition of freshly prepared analyte solution (5 mmol/L). The mixed solution was stirred at constant rate during the experiment to maintain its homogeneity.

Calculation details

The possible binding sites of NIT in HOF-22 were calculated by conventional grand canonical monte carlo, using the Sorption program in Materials Studio software. The simulation boxes contain 1 × 4 × 1 unit cells. The Metropolis method was used in all simulation processes. The long-range electrostatic interactions were dealt with the Ewald summation technique. The vdW interactions were described by a 12–6 Lennard–Jones potential using parameters from the universal force field and a cutoff radius of 14 Å. The charges of HOF-22 were calculated using the charge equilibration (Q_{eq}) method as implemented in Materials Studio. The charges and geometry optimization of NIT were calculated using the density function theory (DFT) method. The DFT calculations are performed with the Dmol3 program in Material Studio software. The Perdew–Burke–Ernzerhof method based on the generalized gradient approximation was used.

Table 1. Crystallographic and refinement parameters for HOF-22.

Empirical formula	$C_{34}H_{36}O_8$
Formula weight	572.63
Temperature (K)	200.00 (10)
Crystal system	Monoclinic
Space group	*I*2/*a*
a (Å)	30.0245 (19)
b (Å)	7.9111 (3)
c (Å)	31.7106 (10)
α (°)	90
β (°)	96.916 (4)
γ (°)	90
Volume (Å^3)	7477.3 (6)
Z	8
ρ_{calc} (g/cm^3)	1.017
μ (mm^{-1})	0.590
F(000)	2432.0
Crystal size (mm^3)	0.04 × 0.03 × 0.02
Radiation	CuKα (λ = 1.54184)
2θ range for data collection (°)	7.662–144.694
Index ranges	$-35 \le h \le 36$, $-6 \le k \le 9$, $-25 \le l \le 38$
Reflections collected	13 500
Independent reflections	7130 [R_{int} = 0.0528, R_{sigma} = 0.0655]
Data/restraints/parameters	7130/1/356
Goodness of fit on F^2	1.044
Final *R* indexes [$I \ge 2\sigma$ (*I*)]	R_1 = 0.1042, wR_2 = 0.2928
Final *R* indexes (all data)	R_1 = 0.1597, wR_2 = 0.3525
Largest different peak/hole (e Å^{-3})	0.68/–0.69

Note: The molecular formula and formula weight were calculated based on the crystal structures without the consideration of guest molecules. Calculation based on the HOF crystal structures using PLATON software. $R_1 = \Sigma(||F_o| - |F_c||)/\Sigma|F_o|$; $wR_2 = [\Sigma w(|F_o|^2 - |F_c|^2)^2/\Sigma w(F_o^2)]^{1/2}$.

Results and discussion

Synthesis, structure, and characterization

H_3CTTA was synthesized through a Suzuki coupling reaction. Recrystallization of H_3CTTA from EtOH afforded needle-shaped crystals suitable for X-ray analysis. X-ray structure determination showed that HOF-22 crystallize in the monoclinic system with the *I*2/a space group. In the crystal structure, the asymmetric unit contains one crystallographic independent H_3CTTA host molecule and two EtOH guest molecules (Supplementary Fig. S1). Two carboxylic groups of one H_3CTTA OBU interact with carboxylic groups of adjacent OBUs through intermolecular O–H···O hydrogen bonds and the third carboxylic group interact with the guest EtOH molecules through an intermolecular C–H···O hydrogen bond instead to form a one-dimensional zigzag chain along *c* axis (Fig. 1*a*). The distances of O–H···O hydrogen bonds are 1.853 and 2.189 Å, respectively, falling into strong hydrogen bond range (Fig. 1*a*). Interestingly, the EtOH molecules can further interact with the adjacent zigzag chain through the intermolecular C–H···C hydrogen bonds to form a two-dimensional (2D) layer (Fig. 1*b*). Three different layers pack together through the intermolecular C–H···O hydrogen bonds to form a 3D framework with one-dimensional (1D) rectangular channel along *b* axis which shows large dimension about 24 × 28 Å^2 (atom to atom distance, Fig. 1*c*). Furthermore, two such frameworks are mutually interpenetrated (Fig. 1*d*). The total solvent-accessible volume in the framework of HOF-22 was estimated to be 33.1% of its unit-cell volume, as estimated by PLATON.[45] The bulky sample of as-synthesized HOF-22 was investigated using PXRD and TGA analysis, confirming its purity and thermal stability. As shown in Supplementary Fig. S2, the experimental PXRD patterns are consistent with those simulated from single-crystal diffraction data, illustrating the phase purity. TGA curve shows that the structure is stable up to approximately 200 °C and a rapid weight loss occurs at 330 °C, indicating the decomposition of the host molecules (Supplementary Fig. S3).

Fig. 1. Crystal structure of HOF-22. (*a*) View of the connection of adjacent OBUs, (*b*) the formation of 2D layer between adjacent zigzag chains, (*c*) the 1D channel in HOF-22 along the *b* axis; (*d*) the two-fold interpenetration of the network, and (*e*) representation of the porous framework (colour code: C, black; O, red; and H, light blue). [Colour online.]

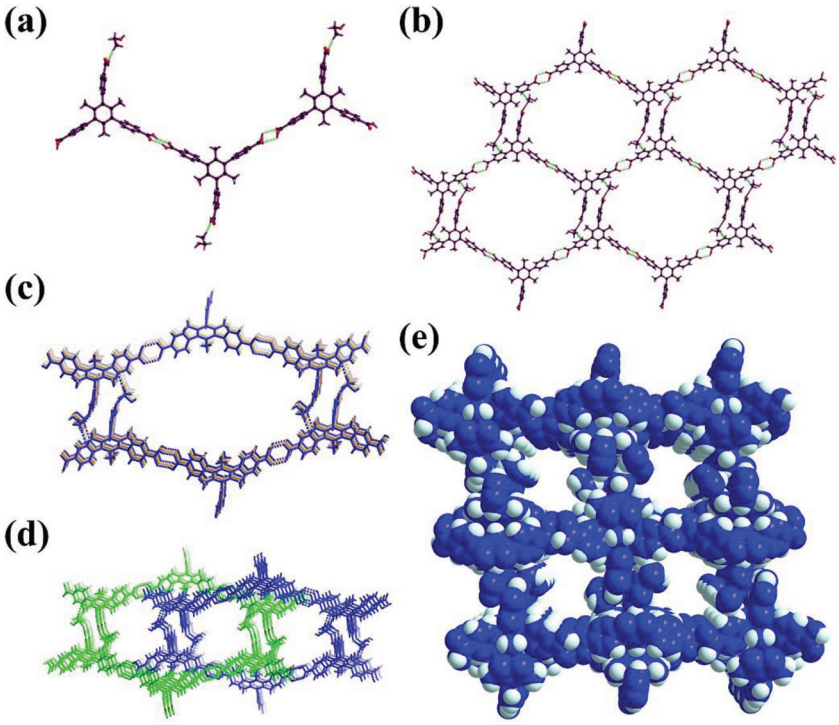

Detection of organic arsenics

Organic arsenics are a kind of antibacterial and growth promoting drug that are usually used as feed additives for animals. As the usage amount on animals increases, the chronic poisoning in humans of organic arsenic and its transformation into inorganic arsenic compounds will cause harmful effects on humans and on the environment. Therefore, the detection of organic arsenic in feed additives and livestock waste is important. Although HOF-22 is soluble in most solvents such as ethanol, methanol, acetone, and ethyl acetate, it is insoluble in water. Moreover, the presence of methyl groups in the central benzene ring of H_3CTTA can efficiently reduce the nonradiative paths by restricting the rotation of benzene rings, making HOF-22 a promising fluorescence material. It should be noted that, because there are no metal ions in the structure of HOF-22, the fluorescence of HOF-22 is ascribed to the organic building unit, H_3CTTA. First, the fluorescence of HOF-22 in water was checked. As shown in Supplementary Fig. S4, it shows good fluorescence in water, which is suitable for sensing some pollutant molecules such as organic arsenics in water. Then, we explored the application of HOF-22 in the detection of organic arsenics based on fluorescent sensing. Here, two representative organic arsenics, ROX and NIT, which are frequently used as feed additives, were selected (Scheme 2).

To explore the ability of HOF-22 to sense a trace quantity of ROX and NIT, fluorescence quenching titrations were performed with the addition of an aqueous solution of organic arsenic to water where HOF-22 is dispersed. As shown in Figs. 2*a* and 2*b*, high fluorescence quenching occurred upon the addition of both ROX and NIT. The quenching efficiencies of ROX and NIT were calculated to be 93% and 97%, respectively, at the highest concentration of the quencher added. In addition, the fluorescence quenching efficiency can be quantitatively described by the Stern–Volmer (SV) equation: $I_0/I = K_{sv}[Q] + 1$, where K_{sv} is the quenching constant ($(mol/L)^{-1}$), [Q] is the molar concentration of the analyte (mol/L), and I_0 and I are the fluorescence intensities before and after addition of the analyte, respectively. As indicated in Figs. 2*c* and 2*d*, the

Scheme 2. Chemical drawings of roxarsone (ROX) and nitarsone (NIT).

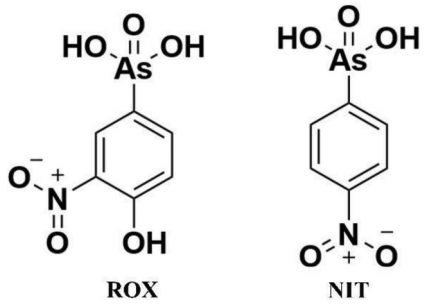

SV plots for ROX and NIT are nearly linear at low concentration range but subsequently deviate from linearity and curve upwards at higher concentrations. The linearity of SV curves for ROX and NIT in low concentration (below 0.25 mmol/L) is good (R^2 = 0.998 and 0.991 for ROX and NIT, respectively; Supplementary Figs. S5 and S6). These nonlinear SV plots might be due to self-absorption or an energy-transfer process. The K_{sv} values of HOF-22 toward ROX and NIT are calculated to be 11 800 and 61 500 $(mol/L)^{-1}$, respectively. Interestingly, as shown in Figs. 2*a* and 2*b*, with the addition ROX, the maximum emission wavelength of HOF-22 shifted to higher wavelength; however, no obvious changes have been observed for the addition of NIT into aqueous solution of HOF-22.

Detection mechanism analysis

To better understand the fluorescence quenching effect of HOF-22 toward ROX and NIT, the quenching mechanism was proposed. Generally, two processes, photoinduced electron transfer (PET) and fluorescence resonance energy transfer (FRET), were considered as the mechanisms for the sensing of organic molecules based on fluorescence quenching method. The PET mechanism is based on the energy level of the lowest unoccupied

Fig. 2. Effect on the emission spectra of HOF-22 dispersed in water upon incremental addition of (*a*) NIT (5 mmol/L) and (*b*) ROX (5 mmol/L) at room temperature; SV curves of (*c*) NIT and (*d*) ROX. [Colour online.]

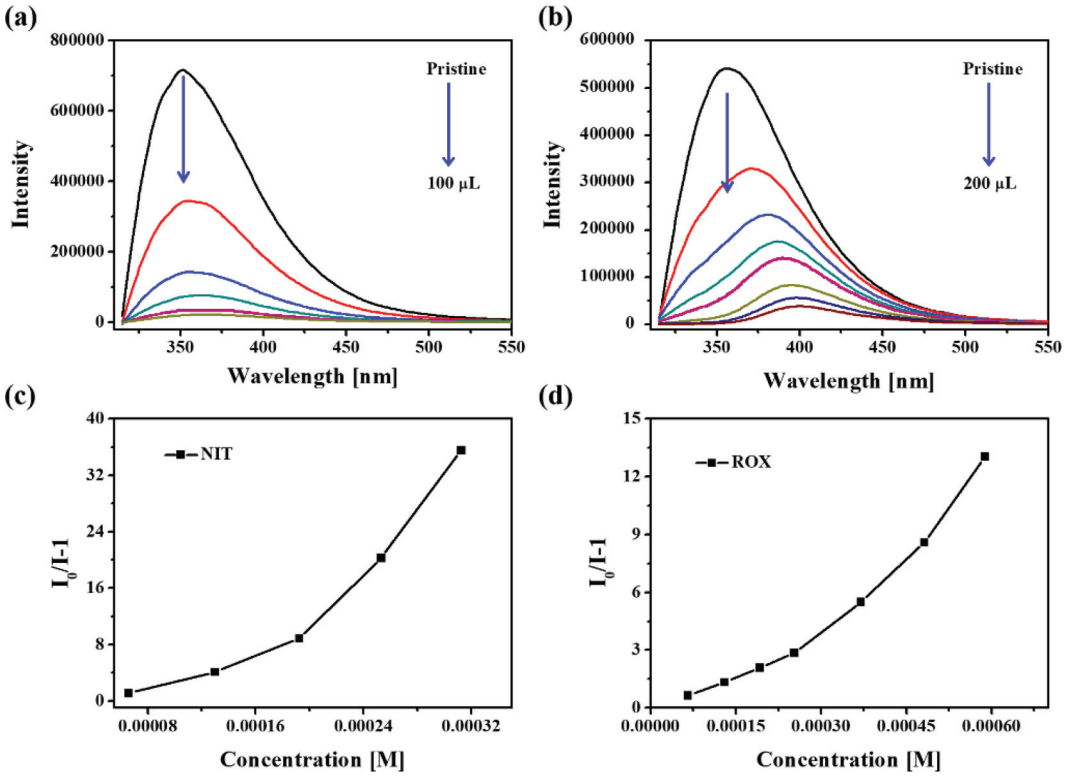

molecular orbital (LUMO) of the HOF and that of the analyte. If the LUMO energy level of HOF is higher than that of analyte, then the PET mechanism occurs. We thus calculated the orbital energies of the LUMOs and highest occupied molecular orbitals (HOMOs) of HOF-22 and tested organic arsenics by DFT calculations (B3LYP/6-31 g*). As shown in Fig. 3*a*, the LUMO energy levels of both ROX and NIT are below that of HOF-22, indicating that PET should be thermodynamically feasible. FRET occurs only when the emission spectrum of the HOF overlaps with the absorption spectrum of the analyte. As shown in Fig. 3*b*, the absorption band of ROX has some degree of overlap with the emission spectrum of HOF-22, indicating the possibility of FRET. However, the absorption of NIT has almost no overlap with the emission spectrum of HOF-22, which means that FRET cannot occur during the detection of NIT. As mentioned above, HOF-22 has excellent detection ability toward both ROX and NIT. Furthermore, the K_{sv} value of NIT is larger than that of ROX, which means that the detection ability of HOF-22 toward NIT is better than that toward ROX. Thus, during the detection of the two organic arsenics, PET is believed to be the primary quenching mechanism.

In addition, as mentioned above, with the addition of ROX, the emission spectrum of HOF-22 shifted to a higher wavelength, and such a phenomenon was not observed during the addition of NIT. In the sensing of ROX using HOF-22 as the sensor, the mechanism was believed to be a combination of the PET and FRET processes. FRET is a long-range process, and the emission quenching is carried over the surrounding fluorophores. PET is a short-range process, and the emission quenching is limited to the fluorophore that has direct interaction with the analytes. Thus, the FRET process is predominant over the PET process. FRET occurs only when the emission spectrum of the HOF overlaps with the absorption spectrum of the analyte. The shift of the fluorescence of HOF-22 should be caused by FRET process. As shown in Fig. 3*b*, the emission spectrum of HOF-22 around 350 nm has large spectral overlaps with the absorption spectra of ROX, whereas the emission spectrum around 400 nm has less overlap with the absorption spectra of ROX. Thus, efficient quenching of the emission spectrum around 350 nm occurs, and the quenching of the emission spectrum around 400 nm occurs only based on a PET process. Thus, the emission spectrum of HOF-22 showed a preferential quench around wavelength of 350 nm. In addition, as shown in Fig. 3*b*, the adsorption spectrum of NIT has very limited overlap with the emission spectrum of HOF-22; thus, the quenching of the emission of HOF-22 by NIT was caused only by the PET process. Thus, spectrum shift was not observed. This phenomenon has been well studied in the sensing of small organic molecules using MOFs as the sensor.[43,46]

Because the electron transfer is a short-range process, the emission quenching by the analytes is limited to the fluorophore that has direct interaction with the analytes, which means that the analytes should form interactions with the framework of HOF-22. To confirm the presence of the weak interactions between the analytes and HOF-22, we carried out a structural optimization on the NIT-loaded HOF-22 by using the Materials Studio Sorption Package. As shown in Fig. 4*a*, the NIT molecules are mainly loaded in the one-dimensional channel of HOF-22, and they can form hydrogen bonding interactions with the framework of HOF-22. As shown in Fig. 4*b*, there are two types of hydrogen bonds between absorbed NIT molecules and organic building units in HOF-22. One is between O atoms of arsenic acid group and H atoms of methyl groups in H_3CTTA with the distance of 2.5 Å; the other one is between O atoms of carboxylic groups in H_3CTTA and H atoms of arsenic acid group with the distance of 2.6 Å.

Conclusions

A new, fluorescent HOF, HOF-22, has been successfully constructed from a tricarboxylic acid OBU and structurally characterized. HOF-22 has potentially applications in the sensing of organic arsenics in water.

Fig. 3. (*a*) HOMO and LUMO energies for HOF-22 and tested organic arsenics arranged in descending order of LUMO energies. (*b*) Overlap between the absorption spectra of organic arsenics and the emission spectra of HOF-22 in water. [Colour online.]

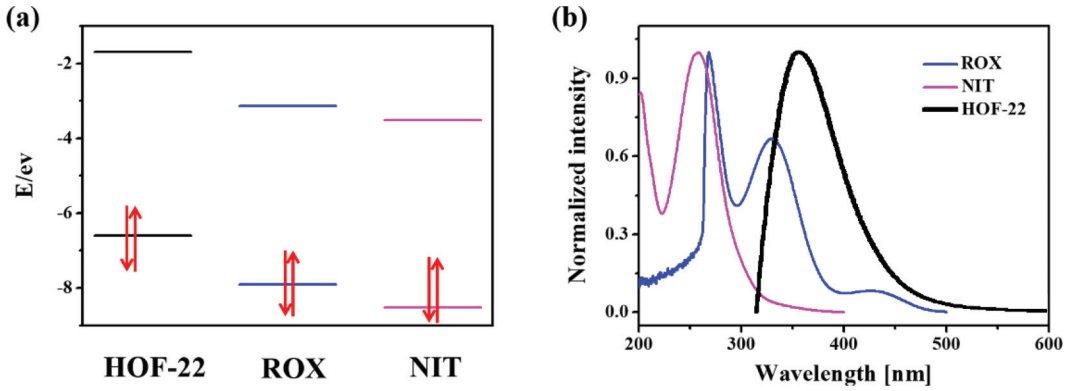

Fig. 4. Crystal structure of NIT-loaded HOF-22. (*a*) NIT adsorption sites in HOF-22 and (*b*) selected fragments highlighting the hydrogen bonding interactions (colour code: C, black; O, red; and H, light blue). [Colour online.]

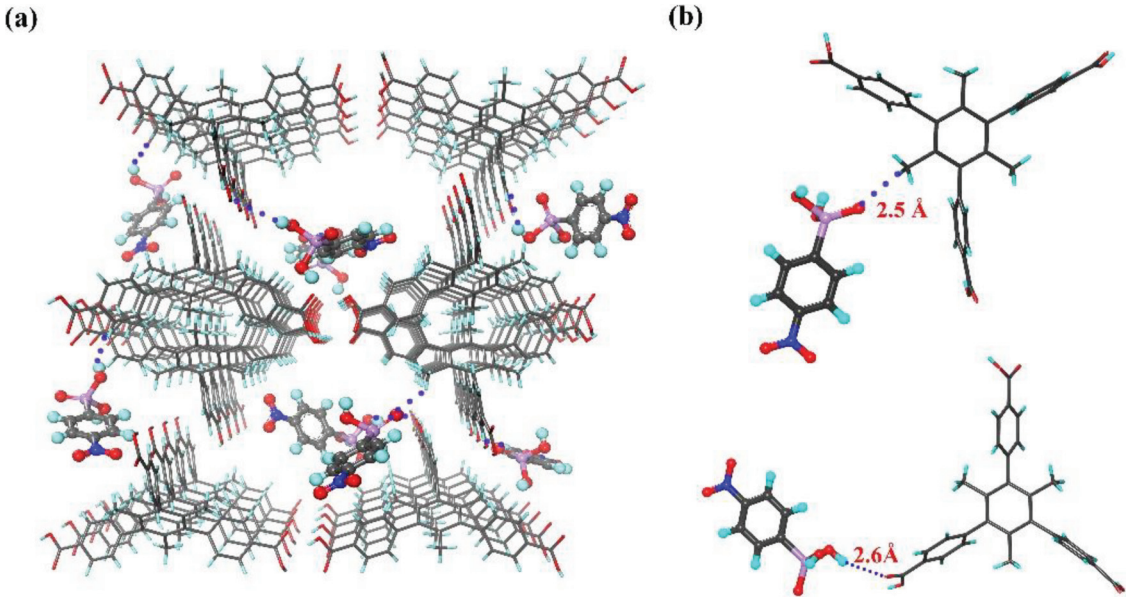

Supplementary data

Supplementary data are available with the article through the journal Web site at http://nrcresearchpress.com/doi/suppl/10.1139/cjc-2019-0417. CCDC 1962363 contains the supplementary crystallographic data for this paper. These data can be obtained, free of charge, via http://www.ccdc.cam.ac.uk/products/csd/request/ (or from the Cambridge Crystallographic Data Centre, 12 Union Road, Cambridge CB2 1EZ, U.K. (fax: 44-1223-336033 or email: deposit@ccdc.cam.ac.uk)).

Acknowledgements

We thank Jing-Hao Liu of Beijing University of Technology for his discussion in computational simulations. We acknowledge financial support from the National Natural Science Foundation of China (Nos. 21731002 and 21975104), China Postdoctoral Science Foundation (grant No. 2018M642556), and the Welch Foundation (AX-1730).

References

(1) Lin, R.-B.; He, Y.; Li, P.; Wang, H.; Zhou, W.; Chen, B. *Chem. Soc. Rev.* **2019**, *48*, 1362. doi:10.1039/c8cs00155c.
(2) Wuest, J. D. *Chem. Commun.* **2005**, 5830. doi:10.1039/b512641j.
(3) Yaghi, O. M. *ACS Cent. Sci.* **2019**, *5*, 1295. doi:10.1021/acscentsci.9b00750.
(4) Cui, H.; Ye, Y.; Arman, H.; Li, Z.; Alsalme, A.; Lin, R.-B.; Chen, B. *Cryst. Growth Des.* **2019**, *19*, 5829. doi:10.1021/acs.cgd.9b00850.
(5) Zhang, X.; Frey, B. L.; Chen, Y. S.; Zhang, J. *J. Am. Chem. Soc.* **2018**, *140*, 7710. doi:10.1021/jacs.8b04277.
(6) Zhang, X.; Zhang, X.; Johnson, J. A.; Chen, Y. S.; Zhang, J. *J. Am. Chem. Soc.* **2016**, *138*, 8380. doi:10.1021/jacs.6b04608.
(7) Cui, H.; Chen, S.; Arman, H.; Ye, Y.; Alsalme, A.; Li, R.-B.; Chen, B. *Inorg. Chim. Acta* **2019**, *495*, 118938. doi:10.1016/j.ica.2019.05.037.
(8) McGuirk, C. M.; Runcevski, T.; Oktawiec, J.; Turkiewicz, A.; Taylor, M. K.; Long, J. R. *J. Am. Chem. Soc.* **2018**, *140*, 15924. doi:10.1021/jacs.8b09631.
(9) Choi, Y.; Noh, K.; Lee, J.; Kim, J. *J. Am. Chem. Soc.* **2018**, *140*, 14586. doi:10.1021/jacs.8b08997.
(10) Li, P.; Li, P.; Ryder, M. R.; Liu, Z.; Stern, C. L.; Farha, O. K.; Stoddart, J. F. *Angew. Chem. Int. Ed.* **2019**, *58*, 1664. doi:10.1002/anie.201811263.
(11) Hashim, M. I.; Le, H. T. M.; Chen, T. H.; Chen, Y. S.; Daugulis, O.; Hsu, C. W.; Jacobson, A. J.; Kaveevivitchai, W.; Liang, X.; Makarenko, T., et al. *J. Am. Chem. Soc.* **2018**, *140*, 6014. doi:10.1021/jacs.8b02869.
(12) Han, B.; Wang, H.; Wang, C.; Wu, H.; Zhou, W.; Chen, B.; Jiang, J. *J. Am. Chem. Soc.* **2019**, *141*, 8737. doi:10.1021/jacs.9b03766.
(13) Nandi, S.; Chakraborty, D.; Vaidhyanathan, R. *Chem. Commun.* **2016**, *52*, 7249. doi:10.1039/c6cc02964g.
(14) Yang, W.; Wang, J.; Wang, H.; Bao, Z.; Zhao, J. C.-G.; Chen, B. *Cryst. Growth Des.* **2017**, *17*, 6132. doi:10.1021/acs.cgd.7b01322.
(15) Yoon, T. U.; Baek, S. B.; Kim, D.; Kim, E. J.; Lee, W. G.; Singh, B. K.; Lah, M. S.; Bae, Y. S.; Kim, K. S. *Chem. Commun.* **2018**, *54*, 9360. doi:10.1039/c8cc04139c.
(16) Hu, F.; Liu, C.; Wu, M.; Pang, J.; Jiang, F.; Yuan, D.; Hong, M. *Angew. Chem., Int. Ed.* **2017**, *56*, 2101. doi:10.1002/anie.201610901.
(17) Hisaki, I.; Suzuki, Y.; Gomez, E.; Cohen, B.; Tohnai, N.; Douhal, A. *Angew. Chem., Int. Ed.* **2018**, *57*, 12650. doi:10.1002/anie.201805472.
(18) Hisaki, I.; Ikenaka, N.; Gomez, E.; Cohen, B.; Tohnai, N.; Douhal, A. *Chem. Eur. J.* **2017**, *23*, 11611. doi:10.1002/chem.201701893.
(19) Hisaki, I.; Nakagawa, S.; Ikenaka, N.; Imamura, Y.; Katouda, M.; Tashiro, M.;

Tsuchida, H.; Ogoshi, T.; Sato, H.; Tohnai, N.; Miyata, M. *J. Am. Chem. Soc.* **2016**, *138*, 6617. doi:10.1021/jacs.6b02968.
(20) Hisaki, I.; Suzuki, Y.; Gomez, E.; Ji, Q.; Tohnai, N.; Nakamura, T.; Douhal, A. *J. Am. Chem. Soc.* **2019**, *141*, 2111. doi:10.1021/jacs.8b12124.
(21) Hisaki, I.; Ikenaka, N.; Tsuzuki, S.; Tohnai, N. *Mater. Chem. Front.* **2018**, *2*, 338. doi:10.1039/c7qm00544j.
(22) Wu, Y. L.; Horwitz, N. E.; Chen, K. S.; Gomez-Gualdron, D. A.; Luu, N. S.; Ma, L.; Wang, T. C.; Hersam, M. C.; Hupp, J. T.; Farha, O. K., et al. *Nat. Chem.* **2017**, *9*, 466. doi:10.1038/nchem.2689.
(23) Yang, W.; Yang, F.; Hu, T.-L.; King, S. C.; Wang, H.; Wu, H.; Zhou, W.; Li, J.-R.; Arman, H. D.; Chen, B. *Cryst. Growth Des.* **2016**, *16*, 5831. doi:10.1021/acs.cgd.6b00924.
(24) Karmakar, A.; Illathvalappil, R.; Anothumakkool, B.; Sen, A.; Samanta, P.; Desai, A. V.; Kurungot, S.; Ghosh, S. K. *Angew. Chem., Int. Ed.* **2016**, *55*, 10667. doi:10.1002/anie.201604534.
(25) Yin, Q.; Zhao, P.; Sa, R. J.; Chen, G. C.; Lu, J.; Liu, T. F.; Cao, R. *Angew. Chem., Int. Ed.* **2018**, *57*, 7691. doi:10.1002/anie.201800354.
(26) Liang, W.; Carraro, F.; Solomon, M. B.; Bell, S. G.; Amenitsch, H.; Sumby, C. J.; White, N. G.; Falcaro, P.; Doonan, C. J. *J. Am. Chem. Soc.* **2019**, *141*, 14298. doi:10.1021/jacs.9b06589.
(27) Desiraju, G. R. *Angew. Chem., Int. Ed.* **1995**, *107*, 2541. doi:10.1002/ange.19951072105.
(28) Malek, N.; Maris, T.; Perron, M. E.; Wuest, J. D. *Angew. Chem., Int. Ed.* **2005**, *44*, 4021. doi:10.1002/anie.200500198.
(29) Chen, T.-H.; Popov, I.; Kaveevivitchai, W.; Chuang, Y.-C.; Chen, Y.-S.; Daugulis, O.; Jacobson, A. J.; Miljanić, O. Š. *Nat. Commun.* **2014**, *5*, 5131. doi:10.1038/ncomms6131.
(30) Zhang, Z.; Lieu, T.; Wu, C.-H.; Wang, X.; Wu, J. I.; Daugulis, O.; Miljanić, O. Š. *Chem. Commun.* **2019**, *55*, 9387. doi:10.1039/c9cc03932e.
(31) Li, P.; He, Y.; Zhao, Y.; Weng, L.; Wang, H.; Krishna, R.; Wu, H.; Zhou, W.; O'Keeffe, M.; Han, Y., et al. *Angew. Chem., Int. Ed.* **2015**, *54*, 574. doi:10.1002/anie.201410077.
(32) Wang, H.; Bao, Z.; Wu, H.; Lin, R. B.; Zhou, W.; Hu, T. L.; Li, B.; Zhao, J. C.; Chen, B. *Chem. Commun.* **2017**, *53*, 11150. doi:10.1039/c7cc06187k.
(33) Wang, H.; Li, B.; Wu, H.; Hu, T.-L.; Yao, Z.; Zhou, W.; Xiang, S.; Chen, B. *J. Am. Chem. Soc.* **2015**, *137*, 9963. doi:10.1021/jacs.5b05644.
(34) Wang, H.; Wu, H.; Kan, J.; Chang, G.; Yao, Z.; Li, B.; Zhou, W.; Xiang, S.; Zhao, J. C.-G.; Chen, B. *J. Mater. Chem. A* **2017**, *5*, 8292. doi:10.1039/c7ta01364g.
(35) Malek, N.; Maris, T.; Simard, M.; Wuest, J. D. *J. Am. Chem. Soc.* **2005**, *127*, 5910. doi:10.1021/ja042233m.
(36) Brunet, P.; Simard, M.; Wuest, J. D. *J. Am. Chem. Soc.* **1997**, *119*, 2737. doi:10.1021/ja963905e.
(37) Brunet, P.; Demers, E.; Maris, T.; Enright, G. D.; Wuest, J. D. *Angew. Chem., Int. Ed.* **2003**, *42*, 5303. doi:10.1002/anie.200352252.
(38) Luo, Y.-H.; Chen, C.; Hong, D.-L.; He, X.-T.; Wang, J.-W.; Ding, T.; Wang, B.-J.; Sun, B.-W. *ACS Appl. Mater. Interfaces* **2018**, *10*, 9495. doi:10.1021/acsami.8b01044.
(39) Li, Y.; Yu, H.; Xu, F.; Guo, Q.; Xie, Z.; Sun, Z. *CrystEngComm* **2019**, *21*, 1742. doi:10.1039/c8ce01800f.
(40) Zentner, C. A.; Lai, H. W. H.; Greenfield, J. T.; Wiscons, R. A.; Zeller, M.; Campana, C. F.; Talu, O.; FitzGerald, S. A.; Rowsell, J. L. C. *Chem. Commun.* **2015**, *51*, 11642. doi:10.1039/c5cc04219d.
(41) Bajpai, A.; Venugopalan, P.; Moorthy, J. N. *CrystEngComm* **2014**, *16*, 4853. doi:10.1039/c3ce42515k.
(42) Bajpai, A.; Venugopalan, P.; Moorthy, J. N. *Cryst. Growth Des.* **2013**, *13*, 4721. doi:10.1021/cg400805c.
(43) Wang, B.; Lv, X.-L.; Feng, D.; Xie, L.-H.; Zhang, J.; Li, M.; Xie, Y.; Li, J.-R.; Zhou, H.-C. *J. Am. Chem. Soc.* **2016**, *138*, 6204. doi:10.1021/jacs.6b01663.
(44) Sheldrick, G. *Acta Cryst.* **2015**, *C71*, 3. doi:10.1107/S2053229614024218.
(45) Spek, A. L. *Acta Cryst.* **2009**, *D65*, 148. doi:10.1107/S090744490804362X.
(46) Nagarkar, S. S.; Joarder, B.; Chaudhari, A. K.; Mukherjee, S.; Ghosh, S. K. *Angew. Chem. Int. Ed.* **2013**, *52*, 2881. doi:10.1002/anie.201208885.